View Article Online
View Journal

Journal of Materials Chemistry C

Materials for optical, magnetic and electronic devices

Accepted Manuscript

This article can be cited before page numbers have been issued, to do this please use: M. Bianchi, S. Carli, M. Di Lauro, M. Prato, M. Murgia, L. Fadiga and F. Biscarini, *J. Mater. Chem. C*, 2020, DOI: 10.1039/D0TC00992J.

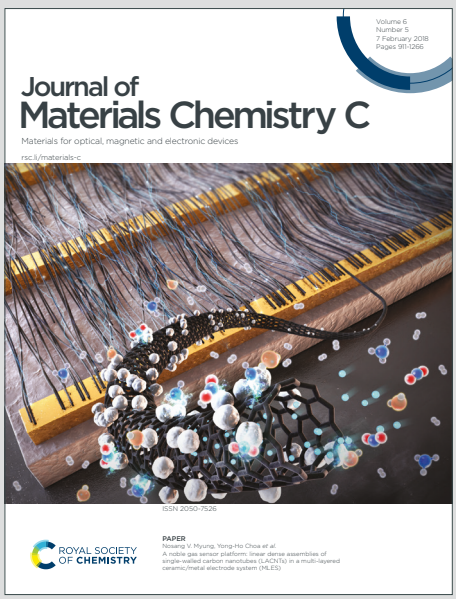

ROYAL SOCIETY OF CHEMISTRY

rsc.li/materials-c

View Article Online
DOI: 10.1039/D0TC00992J

Scaling of Capacitance of PEDOT:PSS: Volume vs Area

Michele Bianchi, Stefano Carli, Michele Di Lauro, Mirko Prato, Mauro Murgia, Luciano Fadiga, and Fabio Biscarini*

Dr. M. Bianchi, Dr. S. Carli, Dr. M. Di Lauro, Dr. M. Murgia, Prof. L. Fadiga, Prof. F. Biscarini
Center for Translational Neurophysiology of Speech and Communication, Italian Institute of Technology, Ferrara 44121, Italy
E-mail: michele.bianchi@iit.it

Dr. M. Prato
Materials Characterization Facility, Italian Institute of Technology, Genova 16163, Italy.

Dr. M. Murgia
Institute for Nanostructured Materials (ISMN), National Research Council, Bologna 40129, Italy

Prof. L. Fadiga
Dipartimento di Scienze Biomediche e Chirurgo Specialistiche, University of Ferrara, Ferrara 44121, Italy

Prof. F. Biscarini
Life Science Department, University of Modena and Reggio Emilia, 41125 (Modena), Italy

Abstract

Poly(3,4-ethylentedioxythiophene):poly(styrenesulfonate) (PEDOT:PSS) is one of the most studied materials for organic bioelectronics, supercapacitors and organic photovoltaics. Its low impedance is ascribed to the so-called volumetric capacitance, a property that phenomenologically correlates the capacitive coupling/charge storage in devices to the PEDOT:PSS volume/thickness. Here we investigate the correlation between the capacitance and the electroactive surface area (ESA) for large-volume spin-cast PEDOT:PSS electrodes. We measure the capacitance with Cyclic Voltammetry (CV) and Electrochemical Impedance Spectroscopy (EIS), and characterize surface morphology by Atomic Force Microscopy and X-ray Photoelectron Spectroscopy. Capacitance of PEDOT:PSS films scales with volume up to ~$5 \cdot 10^6$ μm^3 but saturates

at larger volumes. This scaling behavior is paralleled by the scaling of the ESA, hence the ratio between the effective capacitance and ESA remains constant across the whole data set, thus showing that the specific areal capacitance is indeed the relevant material's property of PEDOT:PSS. EIS data fit supports the experimental evidence obtained by CV, further revealing that the diffusion time constant also saturates at high volumes. This supports the scenario where the effective capacitance relates to the ion accessible ESA, and that the saturation of the capacitance arises from a change of ion penetration from diffusive (at small volumes) to non-diffusive regime at large volumes.

1. Introduction

PEDOT:PSS is one of the most studied conductive polymer for its wide range of applications including solar cells, organic light emitting diodes, organic electrochemical transistors, multi-electrode arrays (MEAs), supercapacitors, and memristors.[1–6] The relevance of PEDOT:PSS arises from the concurrence of attractive chemo-physical properties, such as high conductivity, large capacitance, electrochromism and biocompatibility. Pivotal technological advantages for bioelectronics applications arise from the possibility of being processed from water formulations into thin films using wet deposition techniques, such as spin coating, ink-jet printing, screen printing.[7] Because of its mixed ionic/electronic conduction mode, PEDOT:PSS is the first choice as the signal transducing component in various bioelectronics devices operated in aqueous electrolytes or gels: such as biosensors, electrochemical organic transistors, low-impedance multi-electrode flexible and/or stretchable arrays interfaced with the nervous system, up to neuromorphic logic devices and sensors.[8–13] The mixed ionic-electronic conductivity in PEDOT:PSS results from the presence of two physically distinct, albeit intimately interpenetrated, phases, one being a hole-transport region (the PEDOT-rich phase) and the other being an ion transport region (the PSS-rich phase).[14] This multiscale phase separation occurs from nanometers to mesoscopic length scales. The consequent formation of the electrical double layer at the interface between these two domains gives rise to the large effective capacitance that is one of the most desirable properties of PEDOT:PSS.[15] The linear correlation

View Article Online
DOI: 10.1039/D0TC00992J

between the electrochemical capacitance C and the PEDOT:PSS volume was reported, in a range of small polymer volumes (up to ~ 10^5 μm^3) which is representative of those used in organic electrochemical transistors (OECTs) and micro-fabricated electrodes.[16,17] Following this experimental evidence, the new concept of volumetric capacitance (C*), that is estimated from the slope of the linear C vs volume V, was introduced as the relevant materials parameter. This hints that the whole PEDOT:PSS volume contributes to the effective capacitance.[14] It was however pointed out that possible deviations from this trend may occur at higher polymer volumes, due for instance to incomplete film hydration.[16,18] As technological applications and deposition techniques rely on polymer layers with large thickness/volume, it would be interesting to understand how the capacitance of PEDOT:PSS scales with volume within a larger volume range.[19–22] In particular, all-PEDOT devices, where large volume PEDOT electrodes or free-standing PEDOT:PSS films are printed/deposited on rigid or flexible/biodegradable insulating substrates (such as glass, PDMS, PLGA, PVA or polyesters) are widely investigated for many applications, as chemical sensors, wearable devices, neural probes and bio-hybrid actuating devices.[13,23–26] Therefore, in this work we studied a series of large area (from 4 to 36 mm^2) PEDOT:PSS electrodes prepared by spin coating on an insulating substrate, i.e. glass. Their volume spans two decades, viz 10^5-10^7 μm^3. We characterized film morphology and composition by Atomic Force Microscopy (AFM) and X-Ray Photoelectron Spectroscopy (XPS), and carried out cyclic voltammetry (CV) and Electrochemical Impedance Spectroscopy (EIS) to extract the relevant electrochemical parameters. The aim was to construct the scaling behavior of the capacitance *C* vs *V* and compare it to that of *C* vs the electroactive surface area, ESA. Our main finding here is that the scaling behavior of the capacitance is linearly mirrored by the scaling of the electroactive area, showing that the specific areal capacitance *C*/ESA is indeed a relevant material's property of PEDOT:PSS.

View Article Online
DOI: 10.1039/D0TC00992J

2. Experimental

Materials: PEDOT:PSS solution (Clevios PH1000) was obtained from Heraeus Precious Metals GmbH & Co. (Leverkusen, Germany). The nominal solid content and PEDOT to PSS ratio of the PH 1000 solution were 1−1.3% and 1 : 2.5 by weight, respectively. PEDOT:PSS, 3-Glycidyloxypropyl)trimethoxysilane (GOPS, Sigma-Aldrich, MO, USA) and Dimethyl Sulfoxide (DMSO, Sigma-Aldrich, MO, USA) were used as received without further purification. Borisilicate glass slides (thickness ~ 1 mm, Thermo Scientific, MA, USA) were used as substrate for the deposition of PEDOT:PSS films after ultrasonic cleaning in a mixed solution of pure ethanol, isopropanol and milliQ water (1:1:1 by volume) and drying under sustained flux of pure nitrogen.

Fabrication of the PEDOT:PSS films: PEDOT:PSS thin films were fabricated via a multi-step spin coating procedure. Briefly, a mixture of PEDOT:PSS, GOPS (0.2 % v/v) and DMSO (5 % v/v) was sonicated for 10 min and then filtrated using a filter with nominal pore size of 450 μm (Sartorius Stedim Biotech, France). The following spin coating program was used: 10 s at 300 rpm, 20 s at 600 rpm, 20 s at 2000 rpm. Films were immediately hot-baked (140 °C, 40 min, group A), necessary for a correct consolidation of the PEDOT:PSS layer before the subsequent coating step. Thicker films were fabricated by iterating the spin coating and baking processes up to 4 times, thus obtaining group from B to E (**Figure 1a** and **Figure S1a**). PEDOT:PSS films from group A were used to obtain samples exhibiting smaller volumes (see also "Electrochemical characterization" section). PEDOT:PSS films exhibited an average conductivity of ~ 500 S/cm, obtained according to the Van der Pauw four-point-probe method.[27] In addition, to evaluate the role of the electrode volume aspect ratio, number of processing steps and possible existence of resistive interfaces among the different layers, extra groups were ad-hoc designed (see Figure 3d and Figure S3).

Characterization of film morphology and composition: AFM images were acquired in air at room temperature using a Park XE7 AFM System (Park Systems, Suwon, Korea) operated in

View Article Online
DOI: 10.1039/D0TC00992J

tapping mode. Pre-mounted silicon cantilevers with backside reflecting coating (Al), typical tip curvature radius ~ 7 nm, k ~ 26 N/m and resonant frequency of ~ 300 kHz were used (OMCL-AC160TS, Olympus Micro Cantilevers, Tokyo, Japan). The mean surface roughness (RMS) value was calculated on topographic images of the surface acquired at different scan size (1 x 1, 2.5 x 2.5, 5 x 5 and 10 x 10 μm^2).

XPS spectra were acquired using a monochromatic Al Kα source operated at 20mA and 15kV. High-resolution spectra were collected at a pass energy of 20 eV and an energy step of 0.1 eV, and the Kratos charge neutralizer system was used on all specimens. Spectra were charge corrected to the main line of the C 1s spectrum to 284.8 eV and analyzed with CasaXPS software (Casa Software Ltd., version 2.3.17). Each sulfur species was represented by a S 2p doublet due to spin–orbit coupling. In the fitting procedure, each doublet was fitted to a pair of peaks with the constraints of having the me full width at half maximum, the standard spin–orbit splitting of 1.2 eV, and a statistical branching ratio of 1/2. The position of the S 2p doublet was identified by the position of the most intense component (i.e. the S $2p^{3/2}$ component). All data are shown as mean ± standard deviation.

Electrochemical characterization: all electrochemical measurements were performed in saline ($NaCl_{aq}$ 0.15 M), in a three-electrode cell using a large-area platinum counter electrode (15 x 10 mm), a Ag|AgCl (3 M KCl) reference electrode and the PEDOT:PSS/glass set as the working electrode. All potentials are reported with respect to Ag|AgCl (3 M KCl, +0.197 V vs NHE)[28]. A Kapton mask was placed on PEDOT:PSS films (groups A to E) to define a 6 x 6 mm^2 area to obtain samples with the same geometric area but increasing thickness (Figure 2a, right). In order to extend the series towards smaller volumes, smaller Kapton masks (from 2 x 2 to 5 x 5 mm^2) were placed on samples A. This led to groups A_2x2, A_3x3, A_4x4, A_5x5 (**Figure 3a**, left) exhibiting same thickness but different geometric area. This approach was preferred over direct thickness decrease, since attempts to obtain PEDOT:PSS with smaller thickness than group A resulted into poorly homogenous films. Finally,

View Article Online
DOI: 10.1039/D0TC00992J

PEDOT:PSS/glass electrodes were contacted by using silver paste and kept at a fixed distance (3 mm) from the counter electrode.

Capacitance *C* of the PEDOT:PSS electrodes was extracted by Cyclic Voltammetry (CV) curves using the Equation (1):

$(I_{an}–I_{cat})/2 = C\,\nu$ (1)

where the anodic (I_{an}) and cathodic (I_{cat}) current values were chosen in the current plateau region (at V = 0.3V) and the scan rate ν was set at 25, 50, 75 and 100 mV/s, with the working electrode potential swept between 0 V and + 0.6 V.

The electroactive surface area (ESA), measured in cm^2, was extracted by an independent set of CVs performed in a solution of 10^{-4}M $K_4[Fe(CN)_6]$ in saline. Background CVs were formerly performed in saline at different scan rate (from 25 to 100 mV/s); than CVs were repeated in the Fe^{2+}/Fe^{3+} solutions at the same scan rates. ESA values were obtained by using the Randles–Sevcik equation[29–31] which relates the peak current of the electron-transfer-controlled process with the square root of the scan rate, according to:

$i_p = 2.69\ 10^5\ n^{3/2}\ ESA\ D^{1/2} \cdot S\ \nu^{1/2}$ (2)

Here i_p is the peak current (after subtraction of the capacitive current obtained from the background CVs), S is the concentration of the electroactive species in mol cm^{-3}, n is the number of transfer electrons, D is the diffusion coefficient ($cm^2\ s^{-1}$). The diffusion coefficient (D) of $K_4[Fe(CN)_6]$ was obtained from the slopes of the I_{pa} vs $\nu^{1/2}$ plots using a gold electrode (diameter size: 2 mm, IJ Cambria Scientific Ltd, Llanelli, United Kingdom) as working electrode. For EIS measurements, a sine wave (10 mV RMS amplitude) was superimposed to the working electrode potential of 0 V while varying the frequency from 10^5 Hz to 0.1 Hz. The software ZSimpWin V 3.2 (EChem Software) was used for equivalent circuit modelling of EIS data within the frequency range 1-10^5-Hz, and χ^2 values in the range of 10^{-4}–10^{-6} were used to estimate the goodness of the fit. All data are shown as mean ± standard deviation.

3. Results and Discussion

3.1. Fabrication of PEDOT:PSS films of different thickness.

To obtain large-volume PEDOT:PSS electrodes, Clevios PH1000 thin films of different thickness were first deposited on glass substrate by iterating a combined spin coating and baking process (**Figure 1**a). The average thickness of PEDOT:PSS films increases linearly with the number of spin

View Article Online
DOI: 10.1039/D0TC00992J

coating/baking steps, ranging from ~ 90 nm (sample A, i.e. one step) to ~ 400 nm (sample E, i.e. 5 steps), see Figure 1a. A typical AFM image of surface morphology, shown in Figure 1b, reveals the multiscale organization of nanofibrils (average transversal cross section is 10 - 15 nm) giving rise to local anisotropy within each domain. The domains are not aligned among them, thus resulting in an isotropic assembly. The small scale texture surrounding nano- and mesoscale pores (dark spots whose diameter ranges from 20 - 30 nm) is similarly observed also for the other samples studied (**Figure S1a-d**), suggesting that the underlying layers did not appreciably affect the morphology of the upcoming layer.

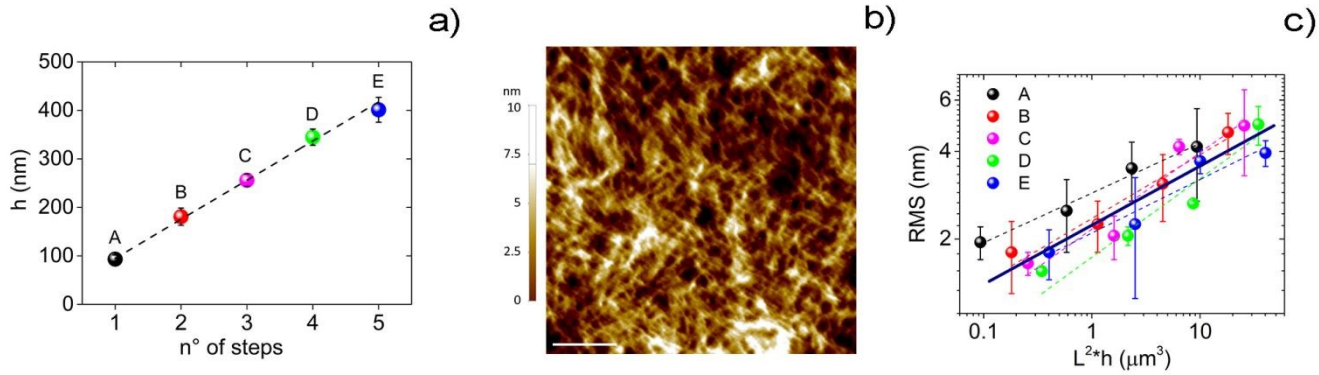

Figure 1. Fabrication and morphological characterization of PEDOT:PSS thin films of different thickness. (a) Mean thickness of PEDOT:PSS films vs. number of spin coating/baking steps (i.e. 1 step: group A; 2 steps: group B; 3 steps: group C; 4 steps: group D; 5 steps: group E) the dashed line represents the linear fit curve; (b) high-resolution AFM topographic images of the surface of a representative PEDOT:PSS film (group E, scale bar is 100 nm); c) RMS roughness vs volume V ($L^2 h$). The dashed lines represent the fitting curves for each group obtained with a power law equation RMS=A L^{α}, whereas the continuous line is the average fitting curve.

All the PEDOT:PSS films showed comparable Root Mean Square (RMS) values, defined as the statistical width of the film surface. The scaling behavior of RMS roughness is considered a universal descriptor apt to classify morphologies that may originate from non-equilibrium phenomena, such as thin film deposition by spin coating. RMS was found to scale monotonically with scan length L and non-monotonically with thickness h (**Figure S2**). We represent this trend by fitting a power law of the image volume $V = L^2 h$: RMS = a V^{β}, as depicted in Figure 1c. The aim of reporting the "volume"

View Article Online
DOI: 10.1039/D0TC00992J

scaling roughness of PEDOT:PSS films is to evaluate possible "outliers" or anomalous samples with a quantitatively different morphology, and likely, not comparable for properties. This care is particularly important when local data from a microscopy are to be correlated with "macroscopic" properties. The fitting curves exhibit best fit values of the pre-factor a and the exponent β ranging respectively from 0.2 ± 0.1 to 0.9 ± 0.1, and from 0.17 ± 0.02 to 0.27 ± 0.06. The global fit yields a = 0.52 ± 0.24 and b = 0.22±0.04. This correlation reveals that the roughness exponent α and dynamic exponent β, associated to self-affine morphology in space (a) and time/mass (b), are entangled/correlated. At the largest L investigated here (10 x 10 μm^2, Figure S2a), RMS tends to saturate at a value of a few nanometers, indicating that spin-cast PEDOT:PSS films were rather flat even on the large scale/small spatial frequencies. Attempts to manufacture thicker films and expand our investigation to higher PEDOT:PSS volumes led to a significant loss of topographic homogeneity and a greater dispersity of surface roughness; for this reason, in this study we investigated films fabricated by up to 5 spin coating cycles. In summary, the combined spin coating and baking process provided PEDOT:PSS films of different thickness that were highly homogenous in terms of morphology.

In **Figure 2,** the results of the XPS characterization carried out on a typical sample of group A are compared with those collected from a sample of group E. The presence of signals from elements of the borosilicate glass substrate (i.e. Ca, Si, Na) was more obvious in the spectra of group A compared to thicker films (Figure 2a). This may indicates that thicker films exhibit the presence of exposed glass which is not properly covered by PEDOT:PSS, and electrons from the uncovered substrate could be excited and reach the XPS detector (for reference, XPS has a typical analysis depth of less than 10 nm). Analysis of the S 2p region can provide useful information for determining the ratio between PSS and PEDOT (R_S/t), given that the two polymers contain one sulfur atom per repeat unit. According to the literature, the S 2p signal at ca.168 eV can be ascribed to the sulfonate groups of PSS whereas sulphur atoms of PEDOT give rise to the peaks at ca. 164 eV (Figure 2b,c).[9]

View Article Online
DOI: 10.1039/D0TC00992J

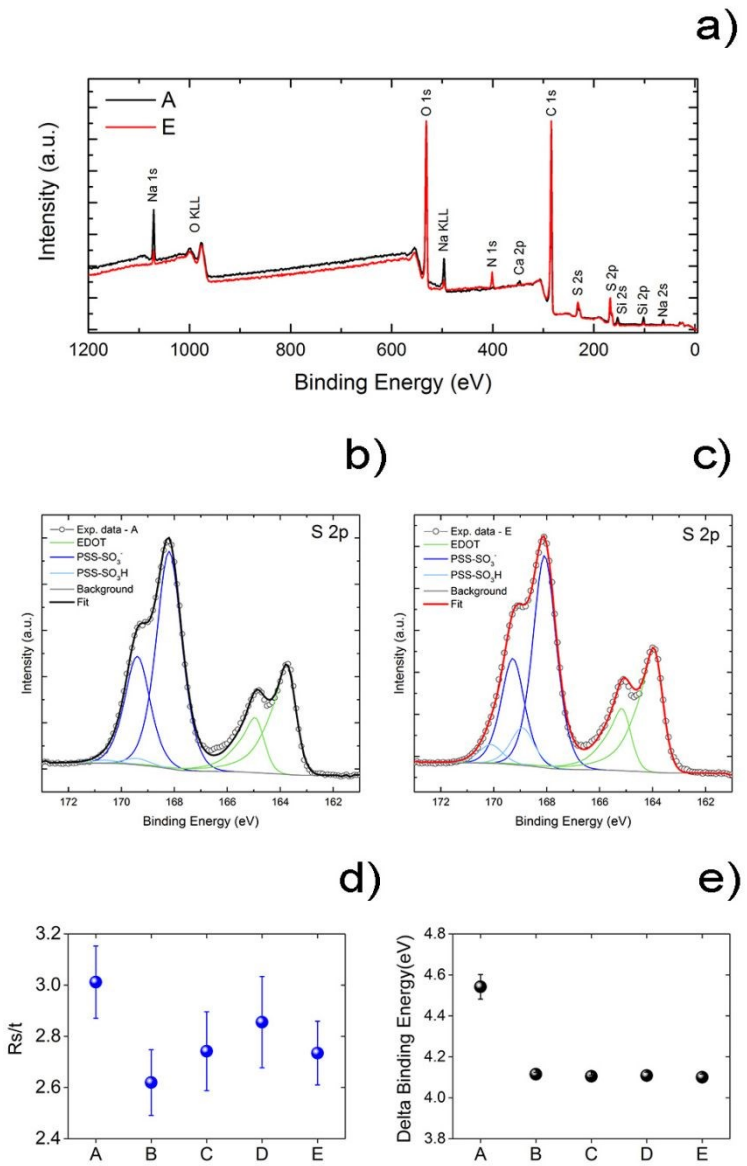

Figure 2. XPS characterization of the PEDOT:PSS films of different thickness. (a) Wide scan collected on PEDOT:PSS electrode for group A and E; b) and c) high-resolution data collected over the S 2p binding energy range for group A and E, respectively; d) ratio between the peak intensity of PSS S 2p (Rs) and PEDOT S 2p (t) for all the groups; e) ratio between the binding energy of PSS S 2p and PEDOT S 2p.

A more deeper analysis of the sulfonates region can been achieved assuming the presence of two different sulfonate species which produce two distinct doublets. In particular, the lower intensity doublet (S 2p main component at ca. 169 eV) can be assigned to the not dissociated sulfonic acid groups SO_3H, whereas the stronger one (S 2p main component at ca. 168.1 eV) accounts for sulfonate

View Article Online
DOI: 10.1039/D0TC00992J

groups SO_3^-. It should be noted that the higher BE observed for SO_3H is linked to the lower charge density around sulfur nucleus, if compared to the negatively charged sulfonate groups.[9] In addition, it is accepted that one positive charge every three monomer units are present in oxidized PEDOT:PSS, which is consistent with a doping ratio on the order of 33 %.[32] Thus, an excess of SO_3H groups is in general observed for chemically prepared PEDOT:PSS and the S 2p signal at higher BE should represent the most intense one.[33] Based on our results, the more intense S 2p signal is localized at the lower BE, and this suggests the presence of an excess of SO_3^- interacting either with the positively charged PEDOT or with other cation species present in the commercial formulation.[33,34]

From the ratio of PSS and PEDOT S *2p* signals, the sulfonate to thiophene proportion in the film can be extracted (Figure 2d). The starting suspension has a PSS to PEDOT ratio of 2.5:1.[35] As can be observed, PEDOT:PSS films deposited by spin coating showed a slightly higher PSS/PEDOT ratio, due to accumulation of PSS at the top surface during the spin coating process, as previously reported.[36] The marginal difference between samples A compared to samples B-E can be ascribed to different segregation of PSS upon the deposition either on the glass substrate (sample A) or on an underlying PEDOT:PSS layer (samples B-E).[37] Similarly, the effect of the glass substrate can be also inferred when considering the slightly different binding energy gap between the main PEDOT and PSS components of the group A and of the other groups (Figure 2e). The observed shift of the PSS-related peaks indicates a different charge density on the sulfonate moieties when the blend is deposited on glass or on a previously grown PEDOT:PSS layer.

3.2. Capacitance of large volume PEDOT:PSS electrodes

In order to evaluate how the electrochemical capacitance of PEDOT:PSS scales with the volume, for large volumes of polymers, we built a series of PEDOT:PSS electrodes whose volume V spans across two orders of magnitudes (**Figure 3a**). According to our preparation, the PEDOT:PSS films exhibited volumes from $4\ 10^5$ to $1.5\ 10^7$ μm^3, a few orders of magnitude larger than volumes usually investigated in OECTs.[16] The capacitance scales linearly with volume for small volume electrodes

View Article Online
DOI: 10.1039/D0TC00992J

(**Figure 3d**); while it slows down and saturates for volumes larger than the threshold value V_C, that we extract from the exponential best fit as detailed in the caption of **Figure 3**. The exponential scaling fit encompasses the linear regime described earlier by Rivnay and coworkers in Ref. 16 at small volumes, and the continuous slow down to saturation. In fact, for $V<V_C$ the fitting functional can be approximated to $C \approx C_\infty + A \cdot (1-V/V_c) = C_0 - A\ V/V_c$ which is a straight line with positive slope. This is confirmed by overlaying the data in log-log plot to those reported by Rivnay and coworkers, as in **Figure S3**, that hints to the continuity of the linear trend of the effective capacitance up to the threshold volume $V_c = 4.6\ 10^6\ \mu m^3$. Above the value V_c, the capacitance attains a plateau $C_\infty \approx 0.77$ mF. As consequence of the saturation of capacitance at larger volumes, the volume capacitance $C^*=(C/V)$ must decrease when the linear regime breaks down, viz. for volumes comparable or larger than V_c. We estimate the volumetric capacitance in the linear regime from our best fit parameters as $C^*=|A|/V_c=170\ Fcm^{-3}$, to be compared to $39\ Fcm^{-3}$ in ref. 26. In the saturation regime the volumetric capacitance instead decreases as C_∞/V. For instance, at $1.5\ 10^7\ \mu m^3$, the volumetric capacitance C^* is $62\ F\ cm^{-3}$. Notably, we demonstrated that the scaling of the capacitance is independent from the adopted geometry or number of processing step. In fact, electrodes with the same volume but with different aspect ratio exhibited the same capacitance (Fig. 3d and Figure S3). In addition, we infer that no significant resistive interfaces are formed between two adjacent PEDOT:PSS layers, as samples with multistep process but volume below V_c still comply to the linear scaling of capacitance with the number of layers (Figure S3).

View Article Online
DOI: 10.1039/D0TC00992J

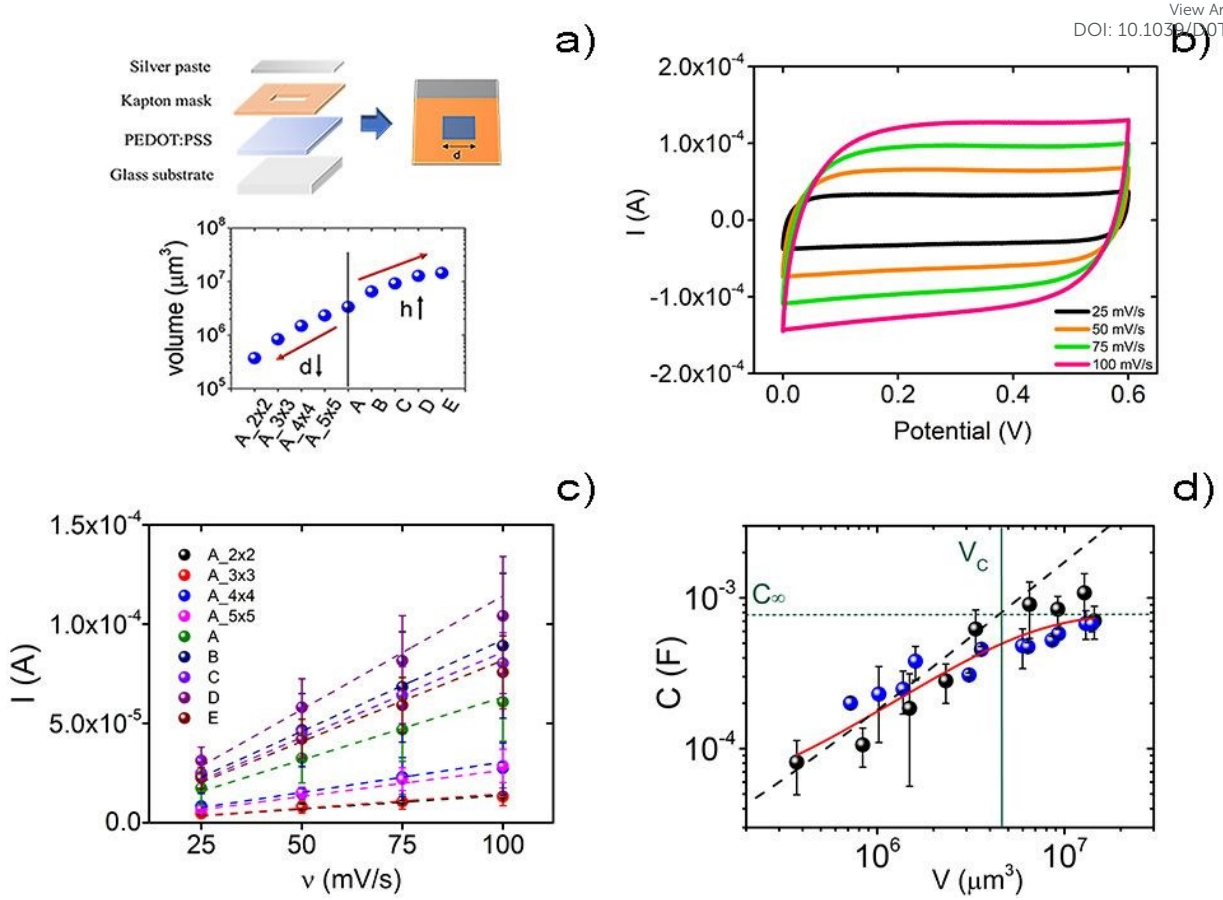

Figure 3. Cyclic voltammetry of PEDOT:PSS films of different volumes. (a) Exploded view of the experimental PEDOT:PSS layout and of the range of investigated PEDOT:PSS volumes obtained by increasing film thickness, *h*, or decreasing the electrode side, *d*; (b) representative CV acquired at different scan rates (on samples of group B); (c) $(I_{an} - I_{cat})/2$, *vs* scan rate for all the investigated groups; dashed lines represent the linear fit whose slope is the capacitance C according to $(I_{an}–I_{cat})/2 = C\,\nu$; (d) Log-log plot of capacitance vs volume for the PEDOT:PSS electrodes investigated in the present study. Extra-groups with volumes built according to different geometry (i.e. area or thickness) were added to the plot (blue markers) to demonstrate that the geometry of the PEDOT:PSS electrode does not affect the final outcome (see Figure S4 for more details about the extra-groups). The dashed red line is our linear fit performed from group A_2x2 to group A (i.e. for $V<V_c$) yielding $C^*=170$ Fcm^{-3}. Best-fit parameters obtained by fitting all data with $C(V)=C_\infty+A\cdot\exp(-V/V_c)$ are $C_\infty= 7.7\ 10^{-4}$ F, $A=C_0 - C_\infty =-7.3\ 10^{-4}$ F, $C_0=C(V=0)\approx0$ and the crossover volume (threshold) from capacitance scaling to saturation $V_c=4.6\ 10^6\ \mu m^3$.

In **Figure S4**, we confirmed that the geometric area of the Pt CE does not limit the amount of charge supplied, and therefore it does not affect the trend of PEDOT:PSS capacitance with volume.

3.3. Analysis of the electroactive surface area

To acquire further insights on this dual volume scaling of the capacitance, we measured the evolution of the electroactive surface area (ESA) of the PEDOT:PSS films vs volume. ESA values were

View Article Online
DOI: 10.1039/D0TC02992J

obtained from CV curves using the Fe^{2+}/Fe^{3+} redox couple in the electrolyte (**Figure 4**a), according to eq. (2). The linear plots of the peak current vs $\nu^{1/2}$ are shown in **Figure S5.** It is worth noting that ESA quantifies the electrochemically functional electrode area, including its roughness, which is accessible by the electrolyte.

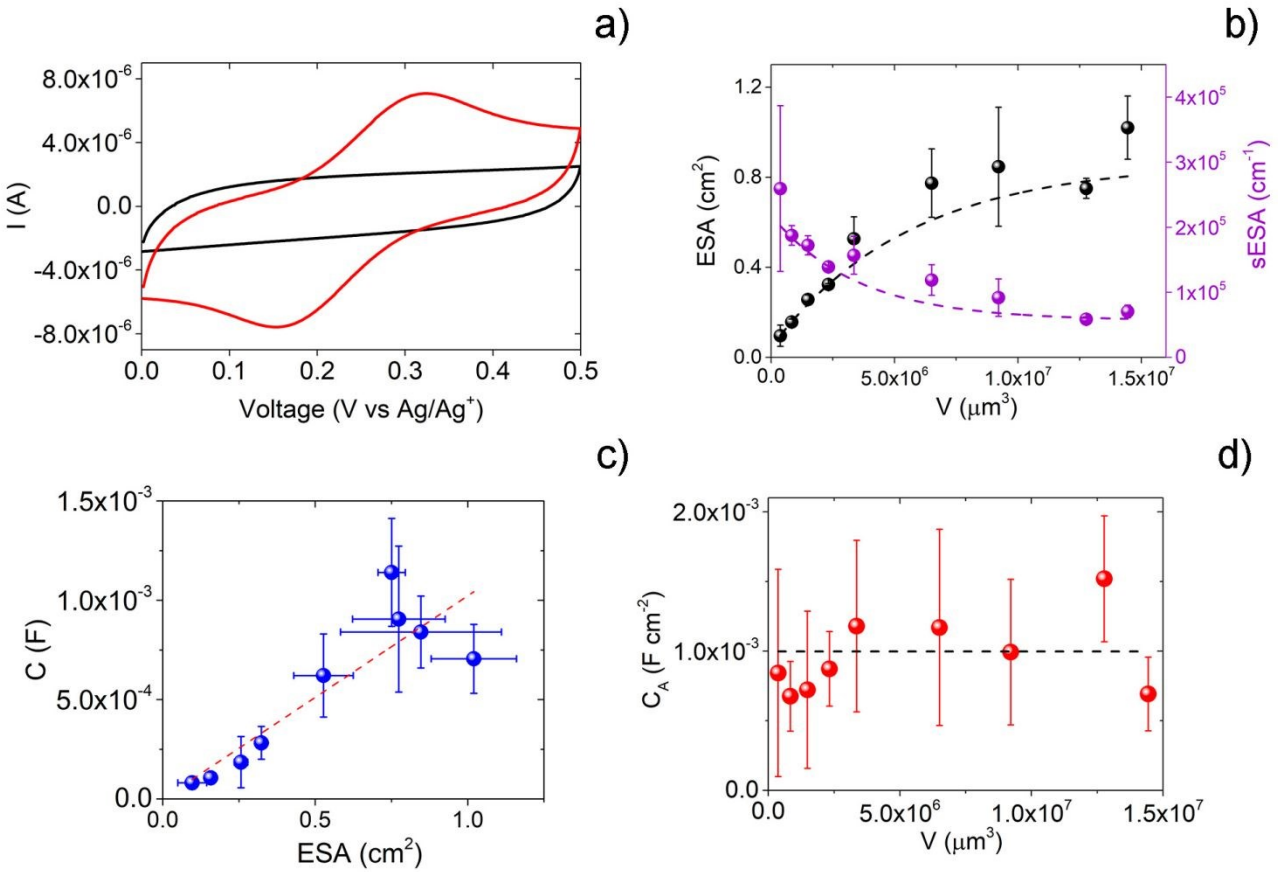

Figure 4. Results of the analysis of the electro-active surface area (ESA) of the PEDOT:PSS electrodes. a) representative CV of PEDOT:PSS in the presence (red line) and absence (black line, for the substraction of the capacitive current) of $[Fe(CN)_6]^{2+/3+}$ (electrolyte 0.1M $NaCl_{aq}$); b) ESA vs. electrode volume (dashed black line is the weighted best fit (R^2 = 0.98, according to $ESA=ESA_\infty+F\exp(-V/V_c)$, with F= -0.82 cm^2, ESA_∞= 0.87 cm^2, V_c = 5.6 10^6 μm^3) and specific ESA (*s*ESA) vs. electrode volume (dashed violet line is the best fit (R^2 = 0.98, according to $sESA=sESA_\infty+G\exp(-V/V_c)$, with G=1.6 10^5 μm^{-1}, $sESA_\infty$= 5.7 μm^{-1}, V_c= 1.1 10^6 μm^3); (c) correlation plot between C and ESA, dashed line is the linear fit (R^2=0.93, slope is 1.0 ± 0.1 mF cm^{-2}); (d) areal capacitance (C_A) vs. electrode volume. Dashed line is the mean value $\langle C_A \rangle$=1.0 10^{-3} F cm^{-2}.

Figure 4b shows the trend of ESA vs volume: ESA scales linearly with V for small electrodes and saturate for larger volumes, thus closely resembling the trend observed for the capacitance. It is

important to stress that the capacitance C and the electroactive surface area ESA were obtained by independent experiments on different sets of samples. In particular C values were extracted both by CV curves in saline and also through independent electrochemical impedance spectroscopy; ESA values were instead extracted from independent CV curves recorded in Fe(II)/Fe(III) solutions. As detailed in the caption of **Figure 4**, the threshold volume V_c=5.6 10^6 μm^3, separating the linearly scaling to the saturated ESA, is comparable to the threshold volume of the capacitance (4.6 10^6 μm^3). Above V_c any further addition of material marginally contributes to ESA. We can now define the specific ESA (*s*ESA) as *s*ESA=ESA/V. *s*ESA is maximum for the smallest electrodes, it then rapidly decreases by increasing the volume of the electrodes, and achieves a plateau for large electrodes. Interestingly, we find a linear correlation between the capacitance and ESA (**Figure 4c**), which strongly hints to the dependence of C from ESA: when ESA saturates also C saturates. Therefore, the property that retains the same value all across the investigated range of PEDOT:PSS volumes is not the volumetric capacitance, but instead the areal capacitance (C_A), defined as the ratio between C and ESA. As can be seen from **Figure 4d**, C_A fluctuates around a mean value equal to (1.0 ± 0.3) mF cm^{-2}. In view of this evidence, C_A appears the invariant material property of PEDOT:PSS.

3.4. Impedance spectroscopy

In order to acquire more insights on the peculiar scaling behavior observed for C and ESA with PEDOT:PSS volume, we carried out EIS measurements and investigated the best fit parameters for the impedance data. As can be observed in **Figure 5a**, the Bode |Z| plot of all the investigated PEDOT:PSS electrodes is characterized by a large frequency independent region at the higher frequencies and a progressive increase of the impedance at the lower frequencies. This trend is typical of PEDOT:PSS which combines both electronic and ionic conductivities.[38] From the linear fitting of Z_{im} (in the low frequency region) vs *1/f*, the capacitance C_{EIS} can be extracted (Figure 5b). Notably, the capacitance value extracted C_{EIS} from the impedance analysis follows exactly the same trend as the capacitance *C* obtained from cyclic voltammetry (see Figure 5 caption for details), hereinafter

View Article Online
DOI: 10.1039/D0TC00992J

explicitly termed C_{CV}. Therefore, the obtained threshold volume V_c (5.2 10^6 μm^3) is comparable to that obtained from CV. The value of the impedance at the highest frequency is commonly associated to the solution resistance R_s. Here, R_s decreases by increasing PEDOT:PSS volume then attains a plateau (Figure 5c, left axis). In particular, R_s scales with $V^{-1/2}$ for samples showing increasing geometric area (i.e. from groups A_2x2 to A), whereas it is only weakly thickness-dependent (i.e. from groups A to E), as previously reported.[17,38,39] It should be also remarked that the trend of R_s mirrors that of ESA reported in Figure 4b, being $R_S \propto \frac{1}{ESA}$.

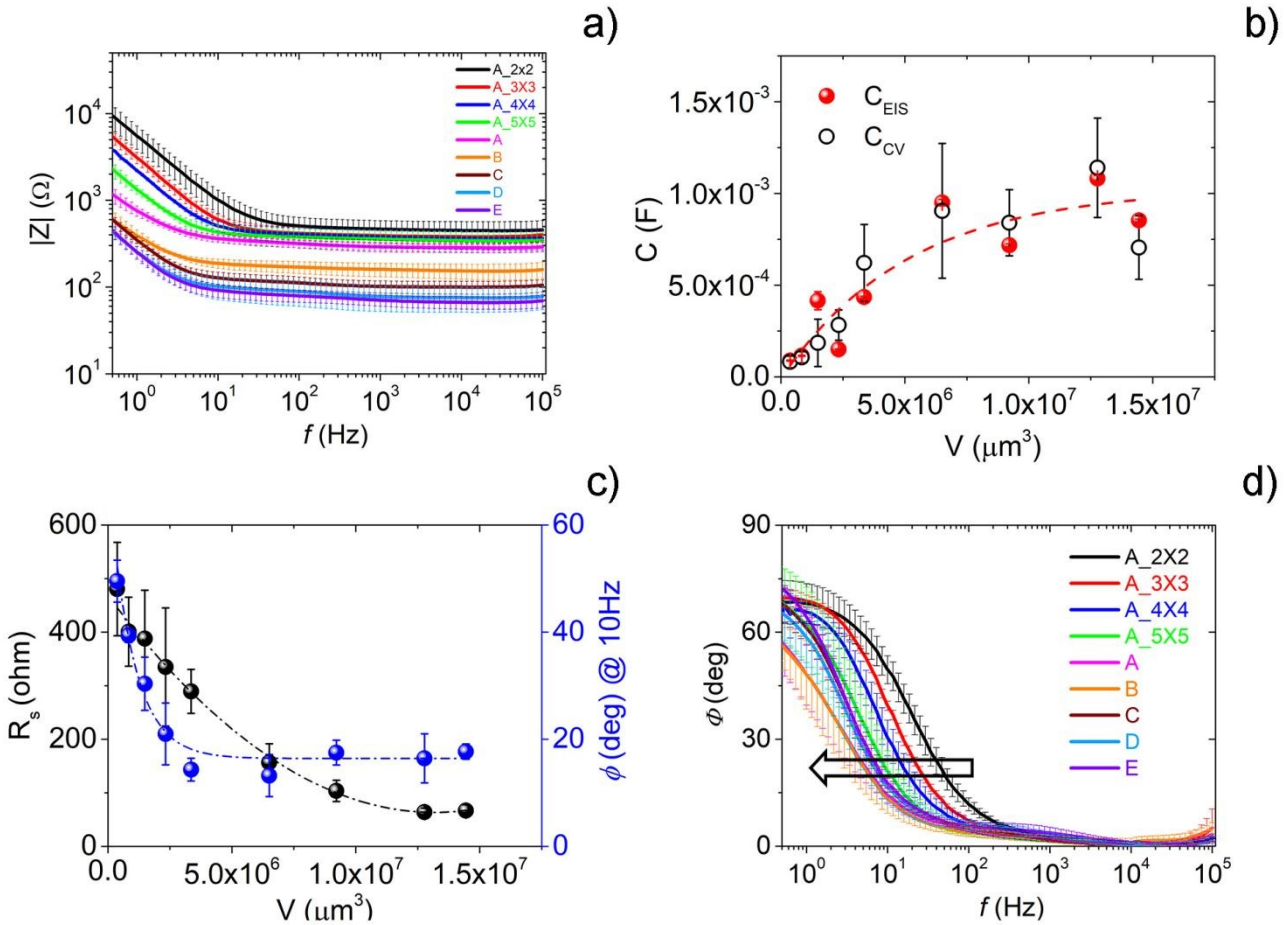

Figure 5. Results of the impedance spectroscopy analysis performed on PEDOT:PSS electrodes with different volume. a) Bode |Z| plot; b) plot of the capacitance, C_{EIS}, extracted from the Bode plot by linear fitting of Z_{im} vs $1/f$ (given that $Z_{im} = 1/(2\pi f\, C_{EIS})$) in the low frequency region (i.e. <10 Hz), compared to the capacitance obtained by CV analysis, C_{CV}. The dashed line is the best fit ($R^2 = 0.85$), according to $C_{EIS}=C_{EIS\infty}+S\cdot\exp(-V/V_c)$, with S=-1.0 10^{-3} F, $C_{EIS\infty}$= 1.0 10^{-3}, V_c = 5.2 10^6 μm^3; c) solution resistance R_s and phase angle ϕ (at 10 Hz) scaling plots vs PEDOT:PSS volume (the blue dash-dotted lines is the guide-for-the-eye lines obtained by fitting R_s data with a parabolic fit,

View Article Online
DOI: 10.1039/D0TC00992J

R^2=0.996, whereas the black dash-dotted line is the guide-for-the-eye lines obtained by fitting phase angle data with an exponential fit, R^2=0.97); d) Bode phase plot (the arrow indicates the widening of the frequency independent region by increasing electrode volume).

In the Bode phase plot (Figure 5d), a progressive broadening of the frequency independent region with increased electrode volume can be observed. The broadening of the frequency independent region, upon increasing of the thickness or area of electrodeposited PEDOT:PSS films or the area of spin cast PEDOT:PSS thin films, has been previously reported.[17,39] Thus, a wider frequency independent region in the Bode |Z| plot of samples prepared through the multi-layer approach (A to E) suggests an optimal charge transport together with good electrochemical communication between the innermost and outermost layers of PEDOT.[17,40,41] Here, the transition from resistive to capacitive behavior falls in the frequency interval of 1-100 Hz. The plot of the phase angle at 10 Hz (Figure 5c, right) indicates a mean (plateau) phase angle of ≈ 15° for larger volumes; below ≈ 5 10^6 μm3, the phase angle increases up to 50° for the smaller electrode volumes. Again, this value is over imposable to the previously obtained threshold volumes. Similar trend was observed for other frequencies encompassing the resistive-capacitive transition (**Figure S6**). Notably, additional impedance measurements carried out at the end of the impedance and CV analyses demonstrated that pre-cycling of PEDOT:PSS was more relevant for smaller volumes rather than for larger ones, excluding possible artefacts due to limited "activation" of larger volumes under the adopted protocol conditions (**Figure S7a**). In addition, evaluation of R_s before and after the electrochemical analyses supported the idea of no electrolyte leakage under the kapton mask (**Figure S7b**), as R_s was found to increase after cycling, and not to decrease as expected in case of leakage.

3.5 Circuit modeling

One of the most used equivalent circuits to fit experimental EIS data for PEDOT:PSS includes a solution resistance R_S in series with the electronic capacitance C_{el} and a finite length Warburg impedance Z_D which relates to ion diffusion through the material pores.[9,38,39] Z_D can be defined as:

View Article Online
DOI: 10.1039/D0TC00992J

$$Z_D = \frac{\tau_D \coth (j\omega\tau_D)^{1/2}}{C_{ion}(j\omega\tau_D)^{1/2}} \qquad (3)$$

where j is the imaginary unit, ω is the angular frequency, τ_D is the diffusional time constant, and C_{ion} is the diffusional pseudocapacitance. A modified version of this circuit foresees the addition of a resistance in parallel with a capacitor to describe fast charge transfer processes at the PEDOT:PSS/electrode interface and/or ion transfer at the PEDOT:PSS/electrolyte interface.[19,41–43] This circuit (see **Figure S8** for a representation), which encompasses a solution resistance R_s in series with a charge transfer element (made by R_{CT} in parallel with C_{CT}), an electronic capacitance C_{el} and Z_D , yielded the best fit for our data (see **Table S1** for the relevant parameters and χ^2 values obtained from the fitting and **Figure S9** for the comparison also with the fitting of the Nyquist plot and of the complex plane capacitance plot with different t circuits.

Analysis of the complex capacitance (**Figure 6**a) outlines the typical feature for an equivalent circuit including R_s in series with a capacitor, i.e. a semicircle on complex plane.[44] The deviation of the fitting from the experimental data that can be observed for the smallest electrodes (Figure 6a, inset), as well as in the corresponding Nyquist plots (Figure S9 c), has been ascribed by Bobacka et al. to the presence of a parallel redox process in very thin PEDOT:PSS films, presumably due to traces of oxygen in the solution.[38] According to the adopted circuit model, the total capacitance is therefore dominated by the two distinct components, namely the electronic capacitance C_{el} and the diffusional pseudo-capacitance C_{ion}, according to the following relationship:

$$\frac{1}{C} = \frac{1}{C_{el}} + \frac{1}{C_{ion}} \qquad (4).^{42}$$

However, C_{ion} exceeds C_{el} of at least one order of magnitude (**Figure S10a** and Table S1), thereby confirming that the total capacitance C is dominated by C_{el}, i.e. by the electronic contribution which relates to the number of charge carriers in the PEDOT film.[38] This outcome is in accordance with previous results obtained for electrodeposited PEDOT films and confirms that the contribution of the diffusional pseudo-capacitance to the total capacitance is negligible also in the range of PEDOT:PSS volumes investigated.[9,38,45] Interestingly, C_{el} saturates at high volumes, affecting the behavior of the

View Article Online
DOI: 10.1039/D0TC00992J

total capacitance (**Figure S10b**). It is worthwhile mentioning that theoretical data of total capacitance vs PEDOT:PSS volume i) are in very good agreement with experimental data obtained by both EIS Bode plot (C_{EIS}) and CV (C_{CV}) analysis (Figure 6b and Table S1), ii) can be fitted with the same exponential fit as C (or equivalently ESA) vs V (see Figure 6 caption for the details), providing a threshold volume (Vc=4.8 10^6 μm^3) similar to those previously obtained.

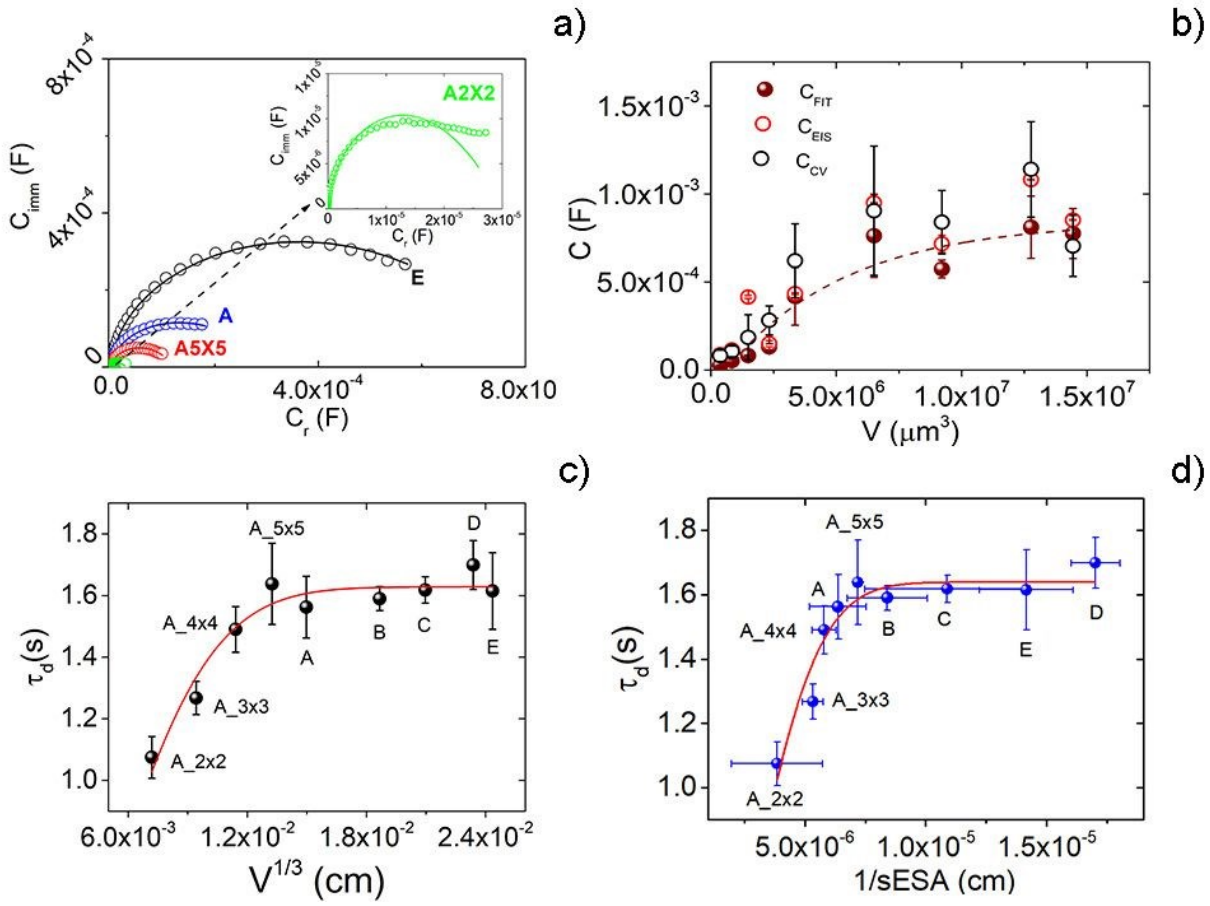

Figure 6. Results from fitting of the EIS data. a) Complex plane capacitance plot for A_2x2 (also magnified in the inset), A5x5, A and E groups (open circles are the experimental data, lines are the fits according to the circuital model in Figure S5); b) comparison among the trend of capacitance extracted from fitting (C_{FIT}), from CV (C_{CV}) and experimental impedance (C_{EIS}) vs PEDOT:PSS volume (the dashed line is the best fit for C_{FIT} data, R^2 = 0.92, according to $C=C_{,\infty}+U\cdot\exp(-V/Vc)$, with U=-9.5 10^{-4} F, C_∞= 8.4 10^{-4}, V_c = 4.8 10^6 μm^3; c) correlation plot between τ_D and $V^{1/3}$. Red line is the best fit (χ^2=3.66) according to eq (5), with, $\tau_\infty = 1.61 \pm 0.03$ s, $\xi = 7.2 \cdot 10^{-3} \pm 0.3 \cdot 10^{-3}$ cm; d) correlation plot between τ_D and 1/sESA. Red line is the best fit (χ^2=6.60) according to eq (6), with $\tau_\infty = 1.62 \pm 0.03$ s, $\xi = 3.9 \cdot 10^{-6} \pm 0.2 \cdot 10^{-6}$ cm=39 ± 2 nm. For plots reported in panels c) and d), the weighted best fit has been performed with Igor Pro 6.3 (Wavemetrics, Lake Oswego, OR) using ξ and τ_∞ as degrees of freedom (DoF) (free parameters).

View Article Online
DOI: 10.1039/D0TC00992J

Despite the fact that the contribution of C_{ion} to the bulk capacitance is negligible, ion diffusion through the pores of PEDOT:PSS certainly plays a key role in determining the final value of the total capacitance. Indeed, the diffusional time constant τ_D is related to the diffusion length L_D and to the diffusion coefficient D according to $\tau_D = \frac{L_D{}^2}{D}$. Therefore, τ_D primarily relies on L_D, which in turn depends on the capability of the electrolyte ions to diffuse inside the material. We have previously defined the specific ESA (sESA) as the ratio between the electroactive surface area ESA and V (Figure 4b). Therefore, for a porous isotropic material, the inverse 1/sESA is the effective thickness of the film if all area was unwrapped on a 2D plane. Another relevant lengthscale considering the isotropic nature of PEDOT:PSS would be $V^{1/3}$. In order to elucidate the nature of the effective L_D that is correlated to τ_D, we plot τ_D vs L_D identified as $V^{1/3}$ and 1/sESA (both lengthscales), (Figure 6c and 6d, respectively). The trends appear similar in scaling: either at low $V^{1/3}$ or at small 1/sESA the trend of $\tau_D$is monotonic then it slows down and/or saturates above a characteristic lengthscale. It is here worth noting that in Figure 6c the crossover occurs between sample group A 5x5 and sample group A, which are samples of same thickness, different areas and made with one step deposition, and not between for instance group A (single-step) and group B (multi-step). In addition, in Figure 6d, one can observed that a few groups swapped their expected position in the plot vs 1/sESA. These observations again support the consideration made regarding the results shown in Figure 3d and Figure S3 concerning the negligible effect of electrode geometry on the observed saturation regime of capacitance and electroactive area. The peculiar trends of τ_D hints to a change of the mechanism that controls the characteristic timescale τ_D. We can envision a diffusive (or sub-diffusive) regime dominating the ion dynamics within PEDOT:PSS in the monotonic increasing branch, which is followed by a non-diffusive mechanism at the onset of the plateau.

The continuous lines in new Figures 6c and 6 d are the best fit lines obtained with the function:

$$\tau_D = \tau_\infty\left[1 - exp\left(-\left(\frac{L_D}{\xi}\right)^\beta\right)\right] \quad (5)$$

View Article Online
DOI: 10.1039/D0TC00992J

This function, which is a stretched exponential, phenomenologically describes a diffusive process that attains a steady state when $L_D > \xi$, ξ being the characteristic length scale. τ_∞ is the large value asymptote. The value of the exponent β identifies a diffusive regime (β =2), sub-diffusive (β <2) or super-diffusive (β =3). To recover the well-known expression for the diffusion equation, one keeps the leading term of the Taylor expansion of eq. 5:

$$\tau_D \approx \left(\frac{\tau_\infty}{\xi^\beta}\right) L_D{}^\beta \quad (6)$$

In eq. 2, for β=2 one recognizes the term in bracket as being the inverse diffusivity D:

$$D = \left(\frac{\xi^\beta}{\tau_\infty}\right) \quad (7)$$

By plugging the best fit values (see caption of Figure 6c) into eq. 7, we obtain D=3.2 10^{-9} $m^2 s^{-1}$ per τ_D *vs* $V^{1/3}$ which is comparable to diffusivity of both Na^+ and Cl^- ions in water.[46] According to Stavrinidou et al. where they measured ion mobilities by the colorimetric monitoring of the displacement of the moving front, the diffusivity of ions in PEDOT:PSS is comparable.[47] This supports the initial ansatz of a slow diffusion in small samples followed different mechanism possibly non diffusive in large samples. Several effects may contribute to the onset of plateau: for instance, electrostatic screening by the ions that progressively occupy the nearest sites, and hence force the later ions to explore longer distances; inhomogenity of chemical composition as Clevios is known to have an excess of PSS, hence PSS rich regions; energy disorder of the ion binding sites.

Although the certain attribution of one or more of these causes to the observed trend requires further experimental evidence, we can envision that only the fraction of the whole PEDOT:PSS volume accessible to electrolyte ions support the establishment of the electrical double layer across the PEDOT and PSS domains, thus contributing to the measured electrochemical capacitance.

4. Conclusions

View Article Online
DOI: 10.1039/D0TC00992J

This work demonstrates that the capacitance of PEDOT:PSS electrodes scaling upon increasing of the electrode volume is a non-monotonic function, where a linear trend is followed by a saturation plateau above a critical volume. This observation demonstrates a correlation of the trend of the capacitance to that of the electroactive surface area, the latter also undergoing saturation above a critical volume, that may be ascribed to the fact that large volume PEDOT:PSS electrodes are not fully accessible to ions of the electrolyte. Interestingly, the critical volume, as extracted from the scaling of different properties measured by independent analyses, is almost invariant. We assume that the observed trend is conserved among different formulations and fabrication approaches. Nevertheless, the critical volume is expected to vary, even sensibly, primarily depending not only on the choice of the PEDOT:PSS formulation but also on the deposition method used (electrodeposition, inkjet printing, spray coating, screen printing), that directly influences material morphology, porosity, surface area, and thus the resulting electrochemical properties. For instance electrodeposited PEDOT:PSS generally exhibit larger roughness than spun coated films other than bumps and pores; we expect then the scaling behavior of electrodeposited films to be shifted also towards larger volumes.

The most important observation here is the invariance of the areal capacitance C_A, which is the ratio between the capacitance and the electroactive surface area. This indicates that the areal capacitance is the figure of merit for assessing the response of the device during operation. The volumetric capacitance instead has a validity restricted to small volume range where PEDOT:PSS is full accessible to ions penetration. The fact that the areal capacitance can be measured with cyclic voltammetry also in combination with impedance spectroscopy, promtps a new proposition for investigating or characterizing OECT (and likely EGOFETs) that enables the separation of the charge mobility from the capacitance in the transconductance extracted from the transfer curves. This would be important to correlate the changes of

transconductance observed, for instance, upon recognition events in OECT sensors, with either a change of capacitance, or to a change in charge mobility or both, thus helping to elucidate the mechanism of capacitive coupling in these devices and to understand how to optimize the device layout for specific bioelectronics operations.

Conflicts of interest

There are no conflicts to declare

References

1 B. Xu and J. Hou, *Adv. Energy Mater.*, 2018, **8**, 1–22.

2 W. H. Kim, A. J. Mäkinen, N. Nikolov, R. Shashidhar, H. Kim and Z. H. Kafafi, *Appl. Phys. Lett.*, 2002, **80**, 3844–3846.

3 S. Inal, G. G. Malliaras and J. Rivnay, *Nat. Commun.*, 2017, **8**, 1–6.

4 L. D. Garma, L. M. Ferrari, P. Scognamiglio, F. Greco and F. Santoro, *Lab Chip*, 2019, **19**, 3776–3786.

5 X. Li, J. Shao, S. K. Kim, C. Yao, J. Wang, Y. R. Miao, Q. Zheng, P. Sun, R. Zhang and P. V. Braun, *Nat. Commun.*, , DOI:10.1038/s41467-018-04937-8.

6 Y. Chen, G. Liu, C. Wang, W. Zhang, R. W. Li and L. Wang, *Mater. Horizons*, 2014, **1**, 489–506.

7 D. T. Simon, E. O. Gabrielsson, K. Tybrandt and M. Berggren, *Chem. Rev.*, 2016, **116**, 13009–13041.

8 Y. H. Kim, C. Sachse, M. L. MacHala, C. May, L. Müller-Meskamp and K. Leo, *Adv. Funct. Mater.*, 2011, **21**, 1076–1081.

9 S. Carli, M. Bianchi, E. Zucchini, M. Di Lauro, M. Prato, M. Murgia, L. Fadiga and F.

View Article Online
DOI: 10.1039/D0TC00992J

Biscarini, *Adv. Healthc. Mater.*, 2019, **1900765**, 1900765.

10 M. Di Lauro, S. Benaglia, M. Berto, C. A. Bortolotti, M. Zoli and F. Biscarini, *Colloids Surfaces B Biointerfaces*, 2018, **168**, 143–147.

11 F. Decataldo, T. Cramer, D. Martelli, I. Gualandi, W. S. Korim, S. T. Yao, M. Tessarolo, M. Murgia, E. Scavetta, R. Amici and B. Fraboni, *Sci. Rep.*, 2019, **9**, 1–9.

12 J. Y. Gerasimov, R. Gabrielsson, R. Forchheimer, E. Stavrinidou, D. T. Simon, M. Berggren and S. Fabiano, *Adv. Sci.*, 2019, **6**, 1–8.

13 M. Giordani, M. Berto, M. Di Lauro, C. A. Bortolotti, M. Zoli and F. Biscarini, *ACS Sensors*, 2017, **2**, 1756–1760.

14 A. V. Volkov, K. Wijeratne, E. Mitraka, U. Ail, D. Zhao, K. Tybrandt, J. W. Andreasen, M. Berggren, X. Crispin and I. V. Zozoulenko, *Adv. Funct. Mater.*, 2017, **27**, 1–10.

15 S. M. Kim, C. H. Kim, Y. Kim, N. Kim, W. J. Lee, E. H. Lee, D. Kim, S. Park, K. Lee, J. Rivnay and M. H. Yoon, *Nat. Commun.*, , DOI:10.1038/s41467-018-06084-6.

16 J. Rivnay, P. Leleux, M. Ferro, M. Sessolo, A. Williamson, D. A. Koutsouras, D. Khodagholy, M. Ramuz, X. Strakosas, R. M. Owens, C. Benar, J. M. Badier, C. Bernard and G. G. Malliaras, *Sci. Adv.*, 2015, **1**, 1–6.

17 D. A. Koutsouras, P. Gkoupidenis, C. Stolz, V. Subramanian, G. G. Malliaras and D. C. Martin, *ChemElectroChem*, 2017, **4**, 2321–2327.

18 J. Newman and W. Tiedemann, *AIChE J.*, 1975, **21**, 25–41.

19 S. Carli, E. Busatto, S. Caramori, R. Boaretto, R. Argazzi, C. J. Timpson and C. A. Bignozzi, *J. Phys. Chem. C*, 2013, **117**, 5142–5153.

20 Y. K. Seo, J. W. Han, K. T. Lim, Y. H. Kim, C. W. Joo, J. Lee, N. S. Cho, S. Yu, M. H.

View Article Online
DOI: 10.1039/D0TC00992J

Kang, C. Yun and B. H. Choi, *Org. Electron.*, 2017, **42**, 348–354.

21 N. Kumar, R. T. Ginting and J. W. Kang, *Electrochim. Acta*, 2018, **270**, 37–47.

22 X. Fan, W. Nie, H. Tsai, N. Wang, H. Huang, Y. Cheng, R. Wen, L. Ma, F. Yan and Y. Xia, *Adv. Sci.*, , DOI:10.1002/advs.201900813.

23 A. Campana, T. Cramer, D. T. Simon, M. Berggren and F. Biscarini, *Adv. Mater.*, 2014, **26**, 3874–3878.

24 I. Gualandi, M. Marzocchi, E. Scavetta, M. Calienni, A. Bonfiglio and B. Fraboni, *J. Mater. Chem. B*, 2015, **3**, 6753–6762.

25 D. Pani, A. Dessi, J. F. Saenz-Cogollo, G. Barabino, B. Fraboni and A. Bonfiglio, *IEEE Trans. Biomed. Eng.*, 2016, **63**, 540–549.

26 F. Greco, A. Zucca, S. Taccola, A. Menciassi, T. Fujie, H. Haniuda, S. Takeoka, P. Dario and V. Mattoli, *Soft Matter*, 2011, **7**, 10642–10650.

27 Y. SINGH, *Int. J. Mod. Phys. Conf. Ser.*, 2013, **22**, 745–756.

28 E. P. Friis, J. E. T. Andersen, L. L. Madsen, N. Bonander, P. Moller and J. Ulstrup, *Electrochim. Acta*, 1998, **43**, 1114–1122.

29 A. J. Bard and L. R. Faulkner, *Electrochemical Methods: Fundamentals and Applications*, Wiley, 2nd edn., 2001.

30 A. R. Harris, P. J. Molino, R. M. I. Kapsa, G. M. Clark, A. G. Paolini and G. G. Wallace, *Analyst*, 2015, **140**, 3164–3174.

31 S. F. Cogan, *Annu. Rev. Biomed. Eng.*, 2008, **10**, 275–309.

32 A. Elschner, S. Kirchmeyer, W. Lovenich, U. Merker and K. Reuter, *PEDOT: Principles and application of an Intrinsically Conducting Polymer*, 2010.

View Article Online
DOI: 10.1039/D0TC00992J

33 G. Zotti, S. Zecchin, G. Schiavon, F. Louwet, L. Groenendaal, X. Crispin, W. Osikowicz, W. Salaneck and M. Fahlman, *Macromolecules*, 2003, **36**, 3337–3344.

34 G. Greczynski, T. Kugler, M. Keil, W. Osikowicz, M. Fahlman and W. R. Salaneck, *J. Electron Spectros. Relat. Phenomena*, 2001, **121**, 1–17.

35 S. Zhang, P. Kumar, A. S. Nouas, L. Fontaine, H. Tang and F. Cicoira, *APL Mater.*, , DOI:10.1063/1.4905154.

36 J. S. Yeo, J. M. Yun, D. Y. Kim, S. Park, S. S. Kim, M. H. Yoon, T. W. Kim and S. I. Na, *ACS Appl. Mater. Interfaces*, 2012, **4**, 2551–2560.

37 H. Djelad, F. Huerta, E. Morallón and F. Montilla, *Eur. Polym. J.*, 2018, **105**, 323–330.

38 J. Bobacka, A. Lewenstam and A. Ivaska, *J. Electroanal. Chem.*, 2000, **489**, 17–27.

39 X. T. Cui and D. D. Zhou, *IEEE Trans. Neural Syst. Rehabil. Eng.*, 2007, **15**, 502–508.

40 Y. P. Kayinamura, M. Ovadia, D. Zavitz and J. F. Rubinson, *ACS Appl. Mater. Interfaces*, 2010, **2**, 2653–2662.

41 S. Carli, E. Castagnola, M. Vomero, A. Scarpellini, M. Prato, N. Goshi, L. Fadiga, D. Ricci and S. Kassegne, *Biointerphases*, 2017, **12**, 031002.

42 P. Danielsson, J. Bobacka and A. Ivaska, *J. Solid State Electrochem.*, 2004, **8**, 809–817.

43 M. Asplund, H. von Holst and O. Inganäs, *Biointerphases*, 2009, **3**, 83–93.

44 M. Itagaki, S. Suzuki, I. Shitanda and K. Watanabe, *Electrochemistry*, 2007, **75**, 649–655.

45 C. Kleber, T. Stieglitz, M. Asplund, U. G. Hofmann, C. Boehler, N. Martini, I. Dryg and Y. Xie, *Biomaterials*, 2017, **129**, 176–187.

46 N. Coppedè, M. Villani and F. Gentile, *Sci. Rep.*, 2014, **4**, 1–7.

47 E. Stavrinidou, P. Leleux, H. Rajaona, D. Khodagholy, J. Rivnay, M. Lindau, S. Sanaur and

G. G. Malliaras, *Adv. Mater.*, 2013, **25**, 4488–4493.

View Article Online
DOI: 10.1039/D0TC00992J

View Article Online
DOI: 10.1039/D0TC00992J

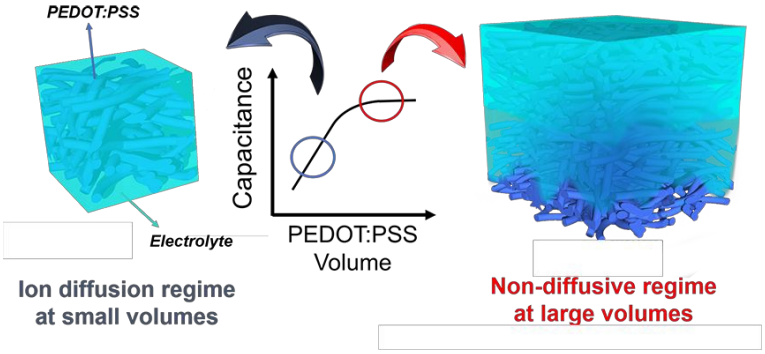

PEDOT:PSS capacitance saturates at large volumes due to a change of ion penetration from diffusive (at small volumes) to non-diffusive regime.